Neutron Imaging at the Oak Ridge National Laboratory: Application to Biological Research

Hassina Z. Bilheux, Jean-Ch. Bilheux, W. Barton Bailey, W. Scott Keener, Larry E. Davis, Ken W. Herwig
Neutron Sciences Directorate
Oak Ridge National Laboratory
Oak Ridge, TN 37831-6475
bilheuxhn@ornl.gov

Maria Cekanova
Small Animal Clinical Sciences
College of Veterinary Medicine, The University of Tennessee
Knoxville, TN 37996
mcekanov@utk.edu

***Abstract*— The Oak Ridge National Laboratory Neutron Sciences Directorate (NScD) has recently installed a neutron imaging beamline at the High Flux Isotope Reactor (HFIR) cold guide hall. The CG-1D beamline supports a broad range of user research spanning from engineering to material research, energy storage, additive manufacturing, vehicle technologies, archaeology, biology, and plant physiology. The beamline performance (spatial resolution, field of view, etc.) and its utilization for biological research are presented. The NScD is also considering a proposal to build the VENUS imaging beamline (beam port 10) at the Spallation Neutron Source (SNS). Unlike CG-1D which provides cold neutrons, VENUS will offer a broad range of neutron wavelengths, from epithermal to cold, and enhanced contrast mechanisms. This new capability will also enable the imaging of thicker biological samples than is currently available at CG-1D. A brief overview of the VENUS capability for biological research is discussed.**

Keywords—neutron imaging; neutron radiography; neutron computed tomography; CG-1D imaging beamline; VENUS; biology

I. Introduction

Neutron imaging [1] is a non-invasive non-destructive technique that is complementary to other imaging techniques such as x-ray/gamma and magnetic resonance (MR) imaging. Neutrons have a zero net charge, and constitute a complementary probe for imaging, interacting with the nucleus of the atom, rather than the electron cloud. Unlike x-rays for which object penetration decreases with the atomic number, the strong interaction forces between neutrons and nuclei do not follow a systematic correlation.

Neutron radiography measures the attenuation of a neutron beam caused by absorption and scattering within a sample, using a two-dimensional position-sensitive detector that measures the transmitted neutron flux. Fig. 1 illustrates the basic layout of a neutron imaging beamline.

This manuscript has been authored by UT-Battelle, LLC, under Contract No. DE-AC05 00OR22725 with the U.S. Department of Energy. The United States Government retains and the publisher, by accepting the article for publication, acknowledges that the United States Government retains a non-exclusive, paid-up, irrevocable, world-wide license to publish or reproduce the published form of this manuscript, or allow others to do so, for United States Government purposes.

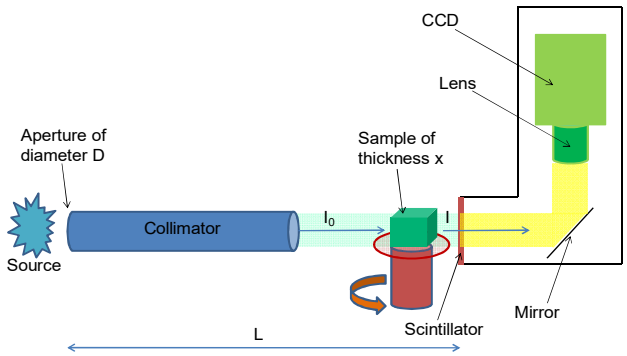

Fig. 1. Layout of a neutron imaging beamline [2].

An aperture of diameter, *D*, is placed after the neutron source and represents the "point" source of the beamline. Size, location and shape of the aperture define the maximum spatial resolution achievable when flight tubes are utilized. The most straightforward layout involves the use of evacuated flight tubes positioned between the aperture and the sample. Optimization of the collimation system may provide uniformity of the beam. The figure of merit of a neutron imaging beamline is L/D, where *L* is the distance from the aperture to the face of the scintillator (where the image is produced). Characterization of a beamline is defined by three properties of the instrument: (1) its flux at sample position, (2) the temporal stability thereof and (3) its divergence.

The beam attenuation caused by a homogeneous uniformly thick sample composed of a single isotope is given by

$$I(\lambda) = I_0(\lambda) e^{-\mu(\lambda)\Delta x} \quad (1)$$

where $I_0(\lambda)$ and $I(\lambda)$ are, respectively, the incident and transmitted beam intensities at wavelength λ, $\mu(\lambda)$ is the attenuation coefficient at wavelength λ and Δx is the thickness of the sample. The attenuation coefficient μ is given by

$$\mu(\lambda) = \sigma_t(\lambda)\frac{\rho N_A}{M} \quad (2)$$

where $\sigma_t(\lambda)$ is the material's total cross section for neutrons of wavelength λ, ρ is its density, N_A is Avogadro's number, and M is the molar mass. **Neutron attenuation, thus attenuation coefficient, depends on the material characteristics and the neutron wavelength, as described in Eq. 2.** In white beam measurements, only the average value of $\sigma_t(\lambda)$ is probed rather than its value at different wavelengths. Wavelength-discrete $\sigma_t(\lambda)$ value can be achieved at neutron pulsed sources by TOF technique [3] or by the use of a monochromatic beam at reactor sources [4], thus enhancing contrast in the object under investigation by varying neutron attenuation.

Straightforward extension of these basic formulae underpins the radiography of heterogeneous and irregularly shaped objects. Due to the interaction properties of neutrons with matter, some light nuclei such as *H*, the most abundant element in biological tissues, greatly scatter neutrons whereas some heavier elements such as *Cu* or *Pb* are not strong scatterers or absorbers of neutrons and can therefore be easily penetrated. A photograph and typical neutron transmission radiograph of a biological tissue is illustrated in Fig. 2. Neutron contrast is mainly due to the presence of *H* atoms.

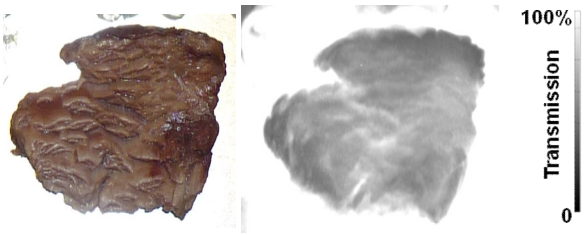

Fig. 2. Representative photograph of 3 mm thick ethanol-fixed skeletal muscle tissue (left) and neutron transmission radiograph (right). The size of the tissue is approximately 2 cm x 2 cm. The tissue was imaged a few minutes after being removed from the fixative solution.

Neutron imaging beamlines have traditionally been installed at reactor-based facilities. These instruments offer (1) a high spatial resolution between 25 to 50 microns on a routine basis, and 15 microns resolution using a micro-channel plate (MCP) detector [5] for a handful of measurements; and (2) a high neutron flux thus permitting low exposure times. Conventionally, neutron radiography (2D) and computed tomography (3D) utilize polychromatic (or white beam) neutron beams in the thermal and cold range. Contrast can be increased when cold neutrons are used, at the expense of a lower transmission, which limits the usable thickness of a biological sample to 2 to 3 mm. The choice of neutron wavelength range is mainly dictated by beam port availability and suitability, detection capability and the anticipated suite of applications at the beamline. Further details on the basics of conventional neutron imaging capabilities, techniques and applications can be found in [2].

II. METHODS

A. The CG-1D Neutron Imaging Beamline

The HFIR CG-1 end location guide on HB4 cold source is occupied by four development beamlines [6]. CG-1A is used for the development of spin-echo resolved grazing incidence scattering (SERGIS) and spin-echo scattering angle measurement (SESAME). CG-1B is a diffractometer for crystal alignment and the development of monochromators. The lower 100 mm of the CG-1 neutron guide is used for neutron imaging measurements. CG-1D is dedicated to neutron imaging, optics and components testing such as imaging detectors.

At CG-1D, apertures (pinhole geometry) are used at the entrance and exit of the He-filled flight path to allow L/D variation from 400 to 2000, with a maximum L of 6.6 m. Samples sit on a translation/rotation stage for alignment and tomography purposes. Detectors for the CG-1D beamline are (1) an ANDOR® DW936 charge-coupled device CCD camera with a field of view of approximately 7 cm x 7 cm and ~ 75 μm spatial resolution, and (2) a MCP detector with a 2.8 cm x 2.8 cm field of view and a 20 microns spatial resolution (in high frame rate mode). Transmitted neutrons are converted to light by the use of a scintillator screen, where they produce a large number of photons. ^{6}LiF/ZnS scintillators of thickness varying from 50 to 200 microns are being used at this facility.

A mirror positioned 45 degrees from the incident beam reflects light to a charge-coupled device (CCD) equipped with a lens.

The CG-1D beamline is illustrated in Fig. 3. The detector assembly was designed to (1) allow easy change of detector components such as scintillator, mirror, CCD and lens and (2) quick and easy translation from the CCD to the MCP detector (30 cm translation) while maintaining good reproducibility in detector position. The CCD assembly is also equipped with integrated lead shielding to reduce gammas mainly produced by the object under neutron investigation. The MCP detector is protected against gammas using a layer of Boron Nitride (BN).

The spectrum at CG-1D, measured using the MCP detector with a flight path of approximately 5.5 m, is displayed in Fig. 4. The guide cut-off is at ~ 0.81 Å and the peak of the spectrum is at ~ 2.6 Å. The "bumps" in the spectrum are due to Aluminum (Al) Bragg edges in the vacuum windows located between the cold source and the detector system.

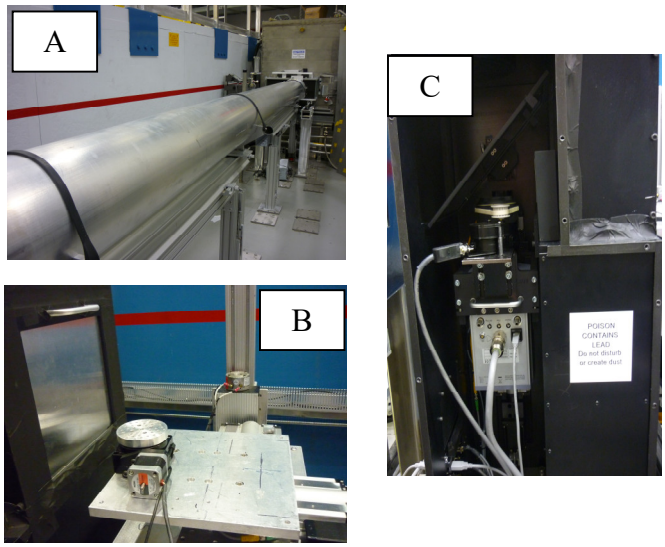

Fig. 3. Photographs of the CG-1D beamline showing the He-filled flight tube (A), detector scintillator next to the rotation stage (B), and CCD housing assembly with mirror, lens and CCD (C).

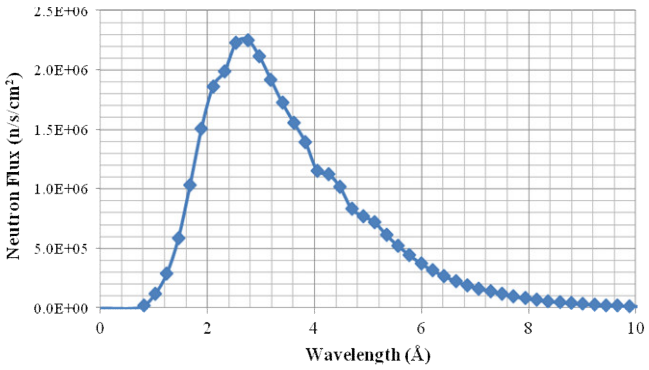

Fig. 4. The CG-1D neutron spectrum is measured with the MCP detector at a flight path distance of approximately 5.5 m, with the chopper running at a frequency 40 Hz and an 5 mm aperture.

B. Neutron Radiography (2D) and Computed Tomography (3D)

The neutron contrast in biological tissues is dominated by neutrons being scattered by H atoms. The radiograph represents a "shadow" image of the neutron interaction with tissues. For 2D imaging, the linear attenuation coefficient, μ, as enunciated in Eq. 1, is averaged over the thickness of the sample so the acquired data do not provide volumetric information. At CG-1D, neutron radiography of biological samples can be performed within 60-120 s. Longer acquisition time might be required when neutron transmission is low. Raw radiographs are normalized using the ORNL in-house iMARS software [7]. Details on normalization procedure can be found elsewhere in these proceedings [8]. Neutron computed tomography (nCT) measures the attenuation of a neutron beam in three dimensions by rotating a sample to record attenuation for multiple beam paths through an object. Usually, the sample is rotated from 0 to 180 degrees, assuming the beam is parallel. Data quality can be improved if the scan is acquired over the full 360 degrees range (super-sampling technique).

Computational reconstruction is performed using the filtered back projection technique (commercial software called Octopus) [9]. Volume rendering of the data set permits visualization of the sample in three dimensions. The information derived from a neutron tomographic data set can be:

- **qualitative**, e.g., observation of the location of a structure within the sample, difference in thickness of bulk material;
- **quantitative**, e.g., bulk material properties, macroscopic transport of a certain material (how much and how fast?), thickness value of a specific material as compared to another one, quantitative response to stimuli (using μ for example), etc.; this information can be obtained by rigorous image analysis of the 2D and 3D data, with careful attention to background correction, data reduction and artifact and scattering corrections [10, 11].

The advantage of nCT is its capability to provide a linear attenuation coefficient anywhere inside the sample, thus enabling in-depth 3D analysis of neutron interactions with the biological sample.

III. RESULTS: NEUTRON RADIOGRAPHY AND COMPUTED TOMOGRAPHY OF BIOLOGICAL SAMPLES

A. Measurements at CG-1D

Several biological tissues have been measured at CG-1D over the past few years. These samples comprised canine and human tissues such as bones, skeletal muscles, kidney, liver, heart, lungs, etc. Fig. 5 displays a typical photograph of a canine kidney (Fig. 5A), and its neutron transmission radiograph in both gray scale (Fig. 5B) and color (Fig. 5C). The tissue provides a contrast while the fat content (marked with an arrow in Figs. 5A and B) is not clearly visible. Fig. 6 illustrates different views of the nCT data of the same kidney slice.

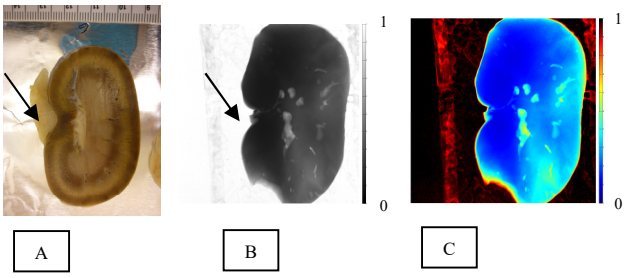

Fig. 5. Two-mm thick canine kidney slice photograph (A), gray-scale (B) and colorized (C) neutron transmission radiographs; using the CCD (spatial resolution ~ 75 μm).

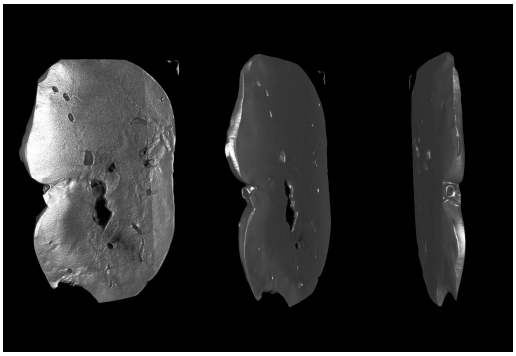

Fig. 6. Volume rendered images computed tomogram of the canine kidney slice from Fig. 5.

B. *Future VENUS capability*

The scientific justification of the Versatile Neutron Imaging Instrument at the SNS (VENUS) is based on the capability of discriminating neutron wavelengths by Time-Of-Flight (TOF) techniques. This offers easy and cost-efficient access to energy selective imaging, hence making use of neutron scattering Bragg-features for improved contrast, strain, texture mapping, and identification of phases in an absorption image. All these techniques have been developed and continue to make significant scientific contributions at reactor-based facilities [4], and more recently at pulsed sources [3]. VENUS will also benefit from a large wavelength spectrum, including more penetrating neutrons than available at CG-1D, enabling the imaging of thicker biological samples (up to several cm) and whole body imaging of small animals such as rodents. The facility will offer two sample positions, at 20 and 25 m, respectively, as illustrated in Fig. 7. The 20-m position will be used for magnification measurements. Anticipated spatial resolution is below 15 µm. The 25-m position will offer a maximum field of view of 28 cm x 28 cm.

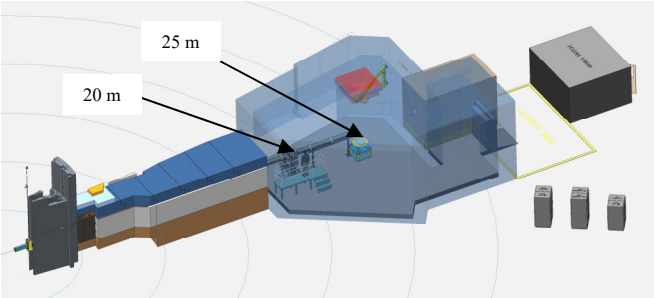

Fig. 7. Layout of the future VENUS facility showing the 20 and 25 m sample position (concentric circle every 5 m from the neutron source).

IV. CONCLUSION

Neutron imaging of biological samples has been demonstrated at the HFIR CG-1D imaging beamline. Contrast is mainly provided by neutrons being scattered by H atoms in the tissue, thus limiting sample thickness to 2-3 mm. The future SNS VENUS facility will allow the imaging of thicker biological samples by using shorter wavelength neutrons (i.e., more energetic neutrons) along with higher spatial resolution.

ACKNOWLEDGMENT

The use of beam line at Oak Ridge National Laboratory's High Flux Isotope Reactor was sponsored by the Scientific User Facilities Division, Office of Basic Energy Sciences, U. S. Department of Energy. The authors would like to thank Mrs. Lakeisha Walker for technical assistance at the CG-1D imaging beamline.

REFERENCES

[1] Ian S. Anderson, Robert L. McGreevy, Hassina Z. Bilheux, Neutron Imaging and Applications, Neutron Scattering Applications and Techniques 01/2009, Springer; DOI:10.1007/978-0-387-78693-3.

[2] J. Nanda, H. Bilheux, S. Voisin, G. M. Veith, R. Archibald, L. Walker, S. Allu, N. J. Dudney,and S. Pannala "Anomalous Discharge Product Distribution in Lithium-Air Cathodes", J. Phys. Chem. C 2012, 116, 8401−8408.

[3] A.S. Tremsin, J.B. McPhate, A. Steuwer, W. Kockelmann, A. M. Paradowska, J. F. Kelleher, J. V. Vallerga, O. H. W. Siegmund, W. B. Feller "High-Resolution Strain Mapping Through Time-of-Flight Neutron Transmission Diffraction with a Microchannel Plate Neutron Counting Detector", Strain 48(4), 296-305.

[4] W. Treimer, M. Strobl, N. Kardjilov, A. Hilger, and I. Manke, "Wavelength tunable device for neutron radiography and tomography", Appl. Phys. Lett. 89 (2006) 203504.

[5] A.S. Tremsin, J.B. McPhate, J.V. Vallerga, O.H.W. Siegmund, W.B. Feller, E. Lehmann, A. Kaestner, P. Boillat, T. Panzner, and U. Filges, "Neutron Radiography with Sub-15 µm resolution through event centroiding", Nuclear Instruments and Methods in Physics Research A 688 (2012) 32-40.

[6] L. Crow, L. Robertson, H. Bilheux, M. Fleenor, E. Iverson, X. Tong, D. Stoica, W. Lee, Nuclear Instruments and Methods in Physics Research A 634 (2011) S71.

[7] iMARS (image Manipulation and Analysis Research Software) is an interactive GUI based on the MatLab® framework.

[8] M. Cekanova, H. Z. Bilheux, J.-C. Bilheux, K. Rathore, R. Donnell, "Neutron Imaging in Cancer Research", these proceedings.

[9] Vlassenbroeck, J., Masschaele, B., Cnudde, V., Dierick, M., Pieters, K., Van Hoorebeke, L. and Jacobs, P. (2010) Octopus 8: A High Performance Tomographic Reconstruction Package for X-ray Tube and Synchrotron micro-CT, in Advances in X-ray Tomography for Geomaterials (eds J. Desrues, G. Viggiani and P. Bésuelle), ISTE, London, UK. doi: 10.1002/9780470612187.ch13

[10] N. Kardjilov, F. de Beer, R. Hassanein, E. Lehmann, and P. Vontobel, Nuclear Instruments and Methods in Physics Research A 542 (2005) 336-341.

[11] R. Hassanein, E. Lehmann, P. Vontobel, Nuclear Instruments and Methods in Physics Research A 542 (2005) 353-360.